Article

Intramolecular Hydrogen Bonding in 1,8-Dihydroxyanthraquinone, 1-Aminoanthraquinone, and 9-Hydroxyphenalenone Studied by Picosecond Time-Resolved Fluorescence Spectroscopy in a Supersonic Jet

Christian Mller, Jrg Schroeder, and Jrgen Troe

J. Phys. Chem. B, **2006**, 110 (40), 19820-19832• DOI: 10.1021/jp0614650 • Publication Date (Web): 24 May 2006

Intramolecular Hydrogen Bonding in 1,8-Dihydroxyanthraquinone, 1-Aminoanthraquinone, and 9-Hydroxyphenalenone Studied by Picosecond Time-Resolved Fluorescence Spectroscopy in a Supersonic Jet†

Christian Müller,*,‡ Jörg Schroeder,‡,§ and Jürgen Troe‡,§

Institut für Physikalische Chemie der Universität, Tammannstr. 6, D-37077 Göttingen, Germany, and Abteilung Spektroskopie und Photochemische Kinetik, Max-Planck-Institut für Biophysikalische Chemie, Am Fassberg, D-37077 Göttingen, Germany

Received: March 9, 2006; In Final Form: April 12, 2006

We investigated spectroscopic and dynamic fluorescence properties of the $S_1 \leftarrow S_0$ transitions of three intramolecularly hydrogen-bonded molecules, 1,8-dihydroxyanthraquinone (1,8-DHAQ), 1-aminoanthraquinone (1-AAQ), and 9-hydroxyphenalenone (9-HPA), by determining their fluorescence excitation spectra and state-selective fluorescence lifetimes under supersonic jet conditions. Moreover, ab initio calculations were performed on one-dimensional hydrogen transfer potential energy curves in both the S_0 and the S_1 state and on S_0 and S_1 minimum energy conformations and normal-mode frequencies at different levels of theory (HF/6-31G(d,p) and B3LYP/6-31G(d,p), CIS/6-31G(d,p) and TDDFT/6-31G(d,p)//CIS/6-31G(d,p), respectively). In line with calculations based on the theory of "atoms in molecules" (AIM), we suggest that the fluorescence properties of 1-AAQ are associated with a single-minimum-type potential. The nonradiative relaxation mechanism is attributed to internal conversion to the S_0 state. For 1,8-DHAQ, we suggest in agreement with previous findings that the fluorescence bands below ~600 cm^{-1} are due to transitions originating in the 9,10-quinone well, whereas the bands above ~600 cm^{-1} are due to transitions originating in the proton-transferred 1,10-quinone well, thus confirming the assumption that 1,8-DHAQ possesses a double-minimum-type S_1 potential. On the basis of our ab initio calculations, we suggest that the fluorescence originating in the 1,10-quinone well is due to vertical absorption into the 9,10-quinone well and subsequent fast ESIPT above the hydrogen transfer barrier. For 9-HPA, only the frequency-domain measurements give tentative evidence of the presence of a pronounced double-minimum-type potential. The rapid nonradiative relaxation mechanism as revealed by fluorescence lifetime measurements is attributed to intersystem crossing to a triplet state.

1. Introduction

Intramolecular hydrogen bonding and the dynamics of intramolecular proton-transfer (PT), or more properly hydrogen-transfer (HT), processes have gained increasing attention in the past two decades for a variety of reasons. The investigation of the ground-state and photoinduced excited-state intramolecular proton transfer (ESIPT) of dihydroxyanthraquinones in general and of 1,8-dihydroxyanthraquinone (1,8-DHAQ)[1−6] in particular has been widely motivated by the need to enhance the understanding of their role as intramolecularly hydrogen-bonded chromophores in anthracycline antitumor antibiotics[7−13] as, for example, adriamycin, aclacinomycin, and daunomycin. Moreover, 1,8-DHAQ is a constituent of the chromophore of hypericin, a polycyclic quinone, which is naturally occurring in St. John's wort (*Hypericum perforatum L.*) and other plants of the *Hypericum* genus. Hypericin displays photoinduced virucidal (anti-viral, anti-retroviral) and antitumor activities and is used as a photosensitizer in photodynamical therapy of cancer.[14] The mechanism of its biological activity is still unclear, but there are indications that an excited-state intramolecular proton transfer could precede the light-dependent intracellular pH decrease leading to the death of the tumor cell by acidification.[15−17]

Alternatively, investigations of the intramolecular hydrogen bond and of the impact of the HT process on static and dynamic properties in the electronic spectroscopy of 9-hydroxyphenalenone (9-HPA)[20−25] aimed at an understanding of genuine quantum mechanical concepts and the application of appropriate quantum mechanical models in molecular physics. Particularly, 9-HPA offered the opportunity to assess the applicability of one-dimensional model potentials as compared to multidimensional potentials in calculating the tunneling splittings of the vibrational ground states in both the electronic ground-state S_0 and the first excited electronic-state S_1. Generally, small model systems possessing intramolecular hydrogen bonds, as for example, 1,8-DHAQ, 1-aminoanthraquinone (1-AAQ), and 9-HPA (Figure 1), are suited for detailed spectroscopic and theoretical investigations of quantum effects associated with the motion of hydrogen atoms. One may investigate the occurrence of vertical/nonvertical cross-well excitations and of dual absorption and fluorescence in the case of asymmetric double-minimum potential energy curves (Figure 2) or the splittings of vibrational ground states in the ground (Δ_0'') and first excited electronic state (Δ_0') due to tunneling in the case of symmetric double-minimum potential energy curves (Figure 3).

We chose our model compounds, 1,8-DHAQ, 1-AAQ,[26−28] and 9-HPA, in an attempt to study systematically the sensitiviy

† Part of the special issue "Charles B. Harris Festschrift".

* Corresponding author. E-mail: cmuelle4@gwdg.de.
‡ Institut für Physikalische Chemie der Universität.
§ Max-Planck-Institut für Biophysikalische Chemie.

10.1021/jp0614650 CCC: $33.50
Published on Web 05/24/2006

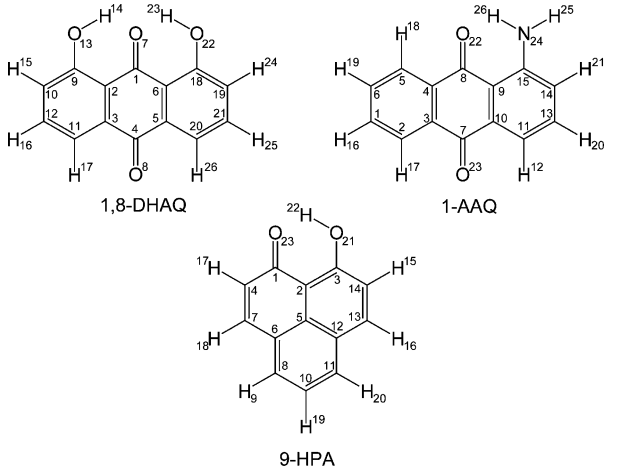

Figure 1. Atom labeling schemes of 1,8-DHAQ, 1-AAQ, and 9-HPA.

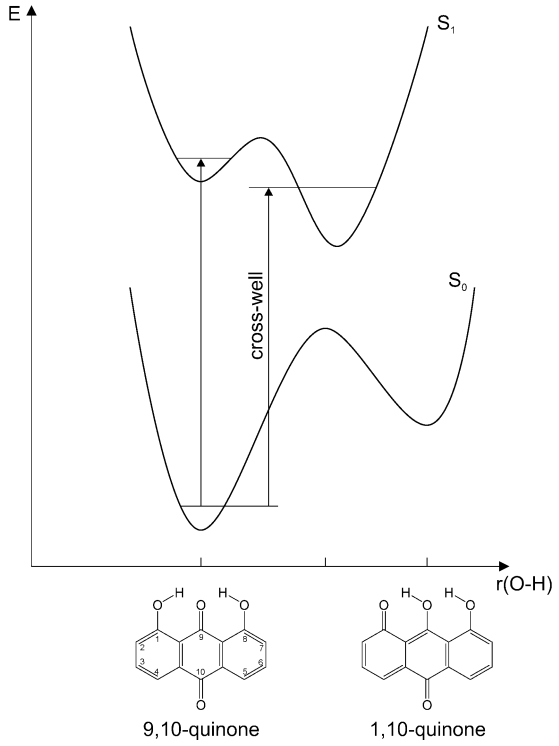

Figure 2. Potential energy diagram of the H-atom transfer in 1,8-DHAQ: asymmetric Lippincott−Schroeder[18,19] potential energy curves.

of spectroscopic and dynamic features on specific intramolecular-hydrogen-bond associated factors. Particularly, we were interested in determining spectroscopic and kinetic evidence of the strength of a particular intramolecular hydrogen bond and the occurrence of excited-state intramolecular proton transfer. Moreover, in an effort to account for our spectroscopic and dynamic findings, we performed ab initio calculations and simulations, which, primarily, aimed at a qualitative understanding of the differences found between the three model systems.

The paper is organized as follows. The experimental setups for measuring fluorescence excitation spectra and fluorescence lifetimes by time-correlated single photon counting (TCSPC) are described briefly in Section 2. In Section 3, the relevant details of our ab initio calculations are summarized. Here we report S_0 and S_1 (for 1,8-DHAQ also S_2) equilibrium geometries and normal-mode frequencies, one-dimensional HT potential energy curves for the respective S_0 and S_1 states calculated on different levels of theory, and, to the best of our knowledge, the first attempt based on the theory of "atoms in molecules"

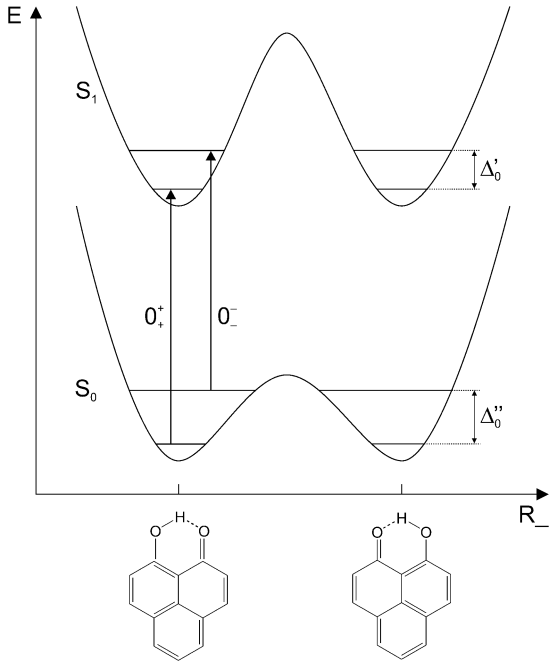

Figure 3. Potential energy diagram of the H-atom transfer in 9-HPA: Symmetric double-minimum potential energy curves. 0_+^+ and 0_-^- are the parity-allowed transitions between the splitted vibrational ground states of the electronic ground (S_0) and the first excited state (S_1).

(AIM)[29−33] to check for a linear relationship between the total charge density $\rho(\mathbf{r}_c)$ at an intramolecular hydrogen-bond critical point and the strength, E_{HB}, of the intramolecular hydrogen bond. With the S_1 HT potential of 9-HPA at hand, we calculate the tunneling splitting of the vibrationless level in S_1. The reliability of the ab initio S_0 equilibrium geometries calculated on the HF/6-31G(d,p) and the B3LYP/6-31G(d,p) level of theory is assessed by comparison with available X-ray diffraction studies[28,34,35] and infrared absorption spectra.[36] In Section 4.1, the fluorescence excitation (FE) spectra of 1,8-DHAQ, 1-AAQ, and 9-HPA are presented and compared with the results of previous studies.[4,25,27] A tentative assignment is given for the vibronic transitions of the FE spectrum of 1-AAQ based on normal-mode frequencies calculated on the CIS/6-31G(d) level of theory. Moreover, the previously reported[4] rotational band contour of the 0_0^0 band origin of 1,8-DHAQ is simulated using the calculated S_0 and S_1 rotational constants. In Section 4.2, the state-selective fluorescence lifetime measurements are presented, which, together with the overall shape of the FE spectra, are analyzed qualitatively in terms of the relative topological properties of the ab initio HT potential energy curves of the ground and the first excited electronic state. The uniform excess energy dependence of the fluorescence lifetimes of 1-AAQ is analyzed quantitatively according to Fermi's Golden Rule.[37,38] Finally, the main results of our present contribution are summarized in Section 5.

2. Experimental Section

The details of the experimental setup for measuring low-resolution fluorescence excitation spectra have been described elsewhere.[39] Therefore, only the relevant features are described here. The jet apparatus consisted of a vacuum chamber evacuated by a diffusion pump (Edwards Diffstak 250/2000M) backed by a rotary pump (Edwards E2M40). The samples were heated to the following temperatures, respectively: 169−174 °C in the case of 1,8-dihydroxyanthraquinone (1,8-DHAQ), 195−200 °C in the case of 1-aminoanthraquinone (1-AAQ),

and 141−144 °C in the case of 9-hydroxyphenalenone (9-HPA). Their vapors were entrained in 3.5−4.0 bar helium and expanded into the vacuum using a General Valve Series 9 nozzle operated in continuous mode. The conically converging nozzle had a smallest orifice diameter of 75 μm in order to maintain a background pressure of about 3.5×10^{-4} mbar. To avoid clogging, the nozzle was heated to the following temperatures, respectively: 209−217 °C in the case of 1,8-DHAQ, 286−305 °C in the case of 1-AAQ, and 188−191 °C in the case of 9-HPA.

For the measurement of the low-resolution fluorescence excitation spectra (Figures 13−15), the molecular beam was crossed at right angle by the parallel polarized beam of a picosecond dye-laser system. The picosecond laser system consisted of a homemade, free jet dye-laser operated in the Runge−Rosenberg configuration,[40] which was synchronously pumped by the frequency-tripled output of a Nd:YVO_4 laser (Spectra Physics, VANGUARD, 355 nm, (10 ± 2) ps pulse duration, 1.0−1.5 W) at a repetition rate of 80 MHz giving pulses with a duration of 7−10 ps at a bandwidth of 1.6−2.5 cm^{-1}. Three different laser dyes were used to make the wavelength range 395−473 nm accessible: Exalite 400E (Exciton, 395−430 nm), Coumarin120 (Lambda Physik, 420−468 nm), and Coumarin47 (Lambda Physik, 420−473 nm). Wavelength calibration was performed with a commercial interferometric wavelength calibration device (Burleigh, Wavemeter WA-5500, accuracy: ±0.2 cm^{-1}).

The horizontally expanding molecular beam was crossed by the laser beam at a distance of about 5 mm downstream of the nozzle. The broadband fluorescence from the interaction region of the crossed molecular and laser beams was collected at right angles to both beams by a *f*/1 collimating lens and focused by a second lens onto the entrance of a microchannel plate photomultiplier (MCP-PMT, Hamamatsu R3809U). The MCP-PMT output was amplified (Hamamatsu C5594) and fed into a constant fraction discriminator (Tennelec TC 454). After passing a second discriminator (Ortec436), the pulses were accumulated in a photon counter (Princeton Applied Research, EG&G Model 1112) and the resulting signal was transferred to a PC. All fluorescence excitation spectra were corrected for the power curves of the dye-laser. However, the intensity differences between the corrected and the uncorrected spectra turned out to be very small.

The fluorescence lifetimes were determined by time-correlated single photon counting using the previously described picosecond dye-laser system for excitation. For time-correlated single photon counting, the output of the MCP−PMT was, as before, amplified and fed into a constant fraction discriminator that delivered the start pulses for a time-to-amplitude converter (TAC, Tennelec TC 862) operated in reversed mode.[41] A second CFD provided the stop pulses, which were derived from a photodiode monitoring the laser output. After subsequent A/D-conversion (Nuclear Data Systems, ND582), the TAC-output was transferred to a PC. The fwhm of the instrument response function was usually about 50−70 ps. For the analysis of the fluorescence decay histograms, a Fourier-transform-based convolution and fitting procedure employing the Levenberg−Marquardt algorithm was used.

The infrared spectrum of 9-HPA (Figure II, available as Supporting Information) was measured in KBr at room temperature with a Perkin-Elmer IR-spectrometer (Series FTIR1600).

1,8-dihydroxyanthraquinone was purchased from Lancaster (99% purity, mp: 191−193 °C), 1-aminoanthraquinone was purchased from Aldrich (97% purity, mp: 253−255 °C), and 9-hydroxyphenalenone was purchased from Synthelec (97% purity, mp: 194−196 °C). All substances were used without further purification.

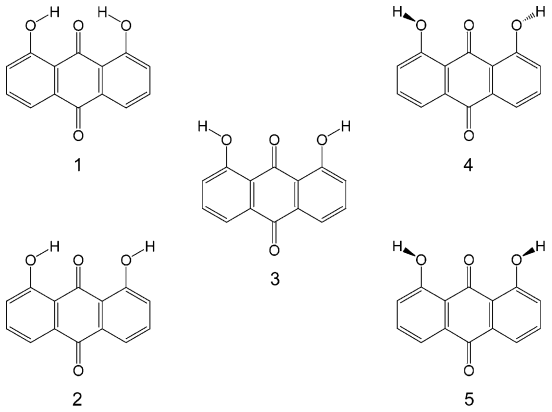

Figure 4. Starting conformations of 1,8-DHAQ for the S_0 geometry optimizations.

3. Computational Details

All calculations were carried out using the GAUSSIAN98 package of programs.[42] Ground-state geometry optimizations were carried out using Hartree−Fock (HF) and density functional theory (B3LYP) methods. Throughout, polarized double-ζ split-valence basis sets (6-31G(d) and 6-31G(d,p)) were used. The optimized minimum energy ground-state geometries served as starting geometries for excited-state optimizations, which were carried out using the configuration interaction method with singly excited configurations (CIS)[43] in combination with the basis sets 6-31G(d) and 6-31G(d,p). All calculated geometries were confirmed to be minimum energy conformations by subsequently checking for the absence of any normal mode with an imaginary frequency. A complete list of the calculated S_0 and S_1 frequencies of 1,8-DHAQ, 1-AAQ, and 9-HPA together with their symmetry species and a numbering of the normal modes according to the numbering scheme of Mulliken[44] and Herzberg[45] is available as Supporting Information (Tables IV−VI).

Different starting conformations of 1,8-DHAQ (Figure 4) were subjected to geometry optimizations in order to determine the most stable S_0 conformer on the B3LYP/6-31G(d,p) level of theory. Conformer1 of C_{2v} point-group symmetry turned out to be the most stable conformer of 1,8-DHAQ in the S_0 state. Conformers 2 and 3 lie higher in energy by ∼4300 cm^{-1} and ∼9300 cm^{-1}, respectively. No stationary point corresponding to a conformer with the H atoms rotated out of plane, neither of C_2 (conformer 4) nor of C_s (conformer 5) symmetry, could be located. Our findings on the destabilization energies of conformers 2 and 3 are in agreement with the previous results of Ferreiro and Rodríguez-Otero,[5] who determined destabilization energies of 14.50 kcal /mol ($\hat{\approx}$5070 cm^{-1}) and 30.30 kcal /mol ($\hat{\approx}$10600 cm^{-1}) for conformers 2 and 3, respectively, on the HF/3-21G level of theory. Conformer 1 of C_{2v} point-group symmetry was also checked to be a minimum energy conformer on the HF/6-31G(d,p) level of theory.

In the case of 1-AAQ, four different conformations (Figure 5) were subjected to geometry optimization in an attempt to determine the most stable S_0 conformation. In contrast to 1,8-DHAQ, the B3LYP/6-31G(d,p) and HF/6-31G(d,p) calculations yielded most stable S_0 conformations of different point-group symmetries. Although the B3LYP/6-31G(d,p) calculation yielded conformer 1 as the only minimum energy conformer, from the HF/6-31G(d,p) calculation conformation 2, containing a slightly

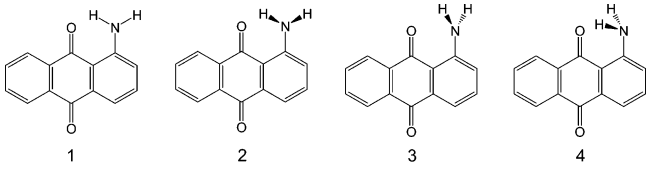

Figure 5. Conformations of 1-AAQ.

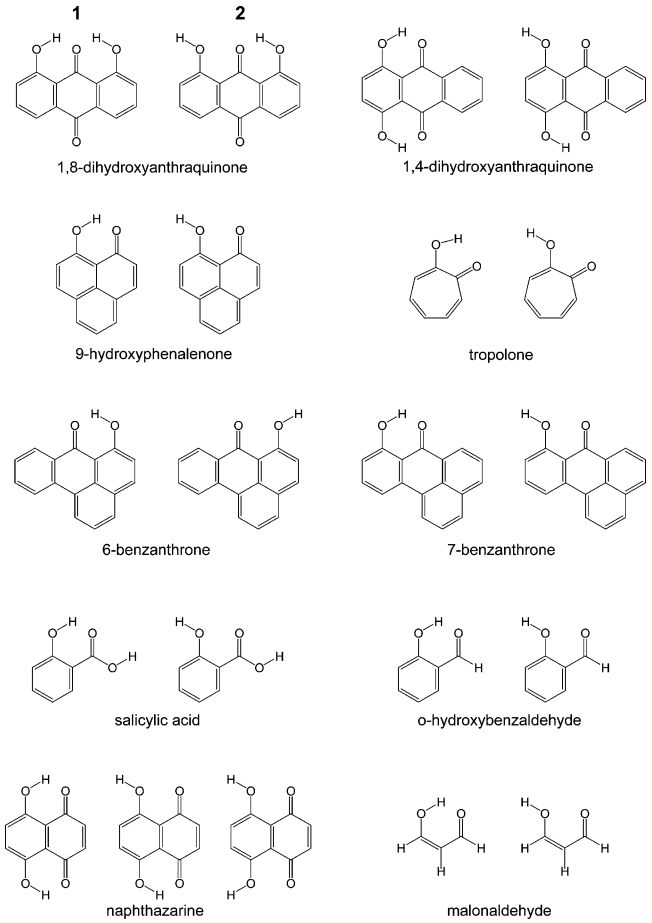

Figure 6. Conformers of the molecules studied according to the theory of atoms in molecules (AIM, see Figure 7).

pyramidalized N atom ($\angle$(9, 15, 24, 26) $\approx$ 10° and $\angle$(14, 15, 24, 25) $\approx$ 13°, see Figure 1), was determined to be solely of minimum energy. Interestingly, we could not confirm the findings of a previous ab initio study on the HF/STO-3G level of theory,[28] which predicted the N and O atom to adopt nonplanar positions on opposite sides of the molecular plane (5° each) and which predicted the central ring to adopt a chair conformation. Our HF/6-31G(d,p) equilibrium conformation exhibits almost complete (quasi-)planarity, only the amino hydrogen atoms lie considerably outside of the molecular plane.

For 9-HPA, two conformations of C_s point-group symmetry (Figure 6, second row) were considered in the attempt to locate the most stable S_0 conformation. Because there obviously is no intramolecular hydrogen bond in conformer 2, it is the less stable conformer destabilized by an energy of $\sim$5100 cm^{-1}.

In an attempt to explain qualitatively the overall time-resolved fluorescence properties of 1,8-DHAQ, 1-AAQ, and 9-HPA presented in Section 4.2, we studied the correlation between the total charge density $\rho(\mathbf{r}_c)$ at the intramolecular hydrogen-bond critical point (3, -1)[29−33] and the hydrogen-bond energy, E_{HB},[5,46] calculated according to

$$E_{HB} = E_{\text{conformer 2}} - E_{\text{conformer 1}} \qquad (1)$$

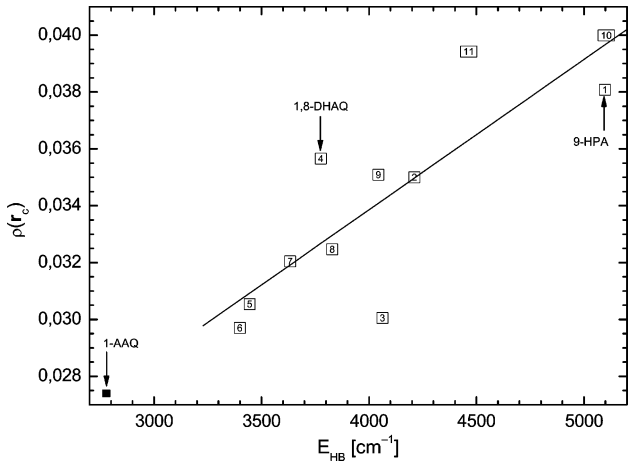

Figure 7. Correlation between the total charge density $\rho(\mathbf{r}_c)$ at the intramolecular hydrogen-bond critical point and the hydrogen-bond energy E_{HB}: [1] 9-hydroxyphenalenone, [2] 1,4-dihydroxyanthraquinone, [3] malonaldehyde, [4] 1,8-dihydroxyanthraquinone, [5] tropolone, [6] *o*-hydroxybenzaldehyde, [7] salicylic acid, [8] naphthazarine (1), [9] naphthazarine (2), [10] 6-benzanthrone, [11] 7-benzanthrone.

where conformer 2 (right) and conformer 1 (left) denote the rotamers of the molecules depicted in Figure 6. Previous studies dealing with AIM topological properties of charge densities reported linear bond-order-bond-length and linear $\rho(\mathbf{r}_c) - E_{HB}$ relationships for covalent CC bonds in hydrocarbons,[47] for intermolecular hydrogen bonds between different nitriles and hydrogen fluoride,[30] different nitriles and hydrogen chloride,[31] different bases and hydrogen fluoride,[32,33] and for multiple-bond critical points as calculated for the van der Waals complexes formaldehyde−chloroform, acetone−chloroform, benzene−formaldehyde, and 1,1-dichloroethane−acetone.[33] All of these studies were carried out on the Hartree−Fock level of theory with different basis sets giving correlation coefficients between $R = 0.869$ and $R = 0.999$.

Our present study is, to the best of our knowledge, the first systematic investigation based on the theory of atoms in molecules attempting to check for a linear $\rho(\mathbf{r}_c) - E_{HB}$ relationship in the case of intramolecular hydrogen bonds. In agreement with previous studies,[30−33] we calculated hydrogen-bond stabilization energies E_{HB} and charge densities $\rho(\mathbf{r}_c)$ at hydrogen-bond critical points on the HF/6-31G(d,p) level of theory. The stabilization energies, E_{HB}, of the molecules given in Figure 6 were determined according to eq 1 from the zero-point energy corrected absolute energies, $E_{\text{conformer 1}}$ and $E_{\text{conformer 2}}$, of the two rotamers, respectively. Calculations concerning the topological properties of the charge density ($\rho(\mathbf{r}_c)$, $\nabla^2\rho(\mathbf{r}_c)$, $|\mathbf{r}_O - \mathbf{r}_c|$ and $|\mathbf{r}_H - \mathbf{r}_c|$) were carried out with the AIMPAC package of programs.[48] Figure 7 shows an approximately linear relationship between $\rho(\mathbf{r}_c)$ and E_{HB}

$$\rho(\mathbf{r}_c)\ [\text{au}] = 5.287 \times 10^{-6}\, E_{HB}\ [\text{cm}^{-1}] + 1.271 \times 10^{-2} \qquad (2)$$

with a correlation coefficient of $R = 0.839$. Correlations between E_{HB} and the Laplacian of the charge density $\nabla^2\rho(\mathbf{r}_c)$, the distance between the O atom and the bond critical point $|\mathbf{r}_O - \mathbf{r}_c|$ or the distance between the H atom and the bond critical point $|\mathbf{r}_H - \mathbf{r}_c|$ are of poorer quality and have correlation coefficients of $R = 0.696$, -0.742, and -0.638, respectively. As is clearly obvious from a comparison of the correlation coefficients, R, the quality of the correlation given in Figure 7 is even worse than that obtained from the investigation of the intermolecular hydrogen bonds between different bases with C, O, N, F, P, S,

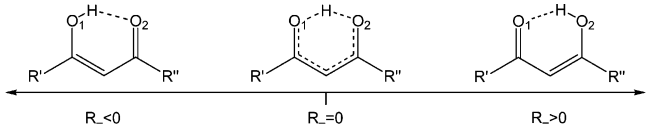

Figure 8. Hydrogen-transfer reaction coordinate R_-.

and Cl acceptor atoms and hydrogen fluoride.[32,33] This outcome, however, can be rationalized as being due to higher sterical constraints in molecules possessing intramolecular hydrogen bonds, especially caused by benzene rings and cata-condensed benzene rings, preventing an optimal structural relaxation of the H-chelate ring. Despite its relatively poor quality, the roughly linear correlation of Figure 7 and eq 2 served to obtain an estimate for the intramolecular hydrogen bond stabilization energy of 1-AAQ. Because no other minimum energy conformation could be located for 1-AAQ, neither on the B3LYP/6-31G(d,p) nor on the HF/6-31G(d,p) level of theory, an estimate of the hydrogen bond strength in 1-AAQ could be obtained only by means of our $\rho(\mathbf{r}_c) - E_{HB}$ correlation. As can be seen in Figure 7, the low charge density at the bond critical point $\rho(\mathbf{r}_c) = 2.74 \times 10^{-2}$ au calculated for 1-AAQ with the HF/6-31G(d,p) electron density at the HF/6-31G(d,p) equilibrium conformation indicates a remarkably weak hydrogen bond. The value of $\rho(\mathbf{r}_c)$ calculated for 1-AAQ is the smallest of all of the molecules studied. This is particularly noteworthy because all other molecules of our survey contained O-atom hydrogen-bond donors. Without having more information to generalize on this point, we conjecture that the H atoms of N−H bonds are involved in weaker intramolecular hydrogen bonds than the H atoms of O−H bonds. We will resort to the calculated relative strengths of the intramolecular hydrogen bonds in Section 4.2.

Finally, in an attempt to account qualitatively for the energy- and time-resolved fluorescence properties of the three model systems under investigation, we determined one-dimensional HT potential energy curves of the ground and the first excited electronic states. We have adopted the coordinate-driven minimum-energy-path (MEP) approach[49−52] for the construction of the reaction path and defined the hydrogen-transfer coordinate R_- (Figure 8) in the usual way as

$$R_- = \frac{R_{O_1H} - R_{O_2H}}{2} \qquad (3)$$

Thus, relaxed potential energy scans were carried out by increasing the bond length R_{O_1H} by steps of 0.02−0.1 Å and optimizing all other internal coordinates (including the bond length R_{O_2H}) in every step.

We decided to determine S_1 minimum energy paths with the CIS method because CIS-optimized reaction paths turned out to provide qualitatively correct characterizations of HT potential energy profiles in the S_1 states of large organic molecules.[51,52] The CIS method, however, is in general unreliable for the prediction of HT barriers in excited electronic states.[50] In agreement with previous studies,[50−52] we, therefore, decided to check the presence of an HT barrier along the reaction path calculated with the CIS method by taking electron correlation via time-dependent density functional theory (TDDFT) into account. Figures 9a, 10a, and 11a display CIS potential energy curves along the HT reaction coordinate R_- as well as TDDFT potential energy profiles calculated on the CIS-optimized MEPs. For a better comparison with the CIS/6-31G(d,p) HT potential energy profiles, the TDDFT results were shifted to higher potential energies $V(R_-)$.

As is clearly discernible, in the case of 1,8-DHAQ and 1-AAQ, the effect of the TDDFT/6-31G(d,p) single point energy

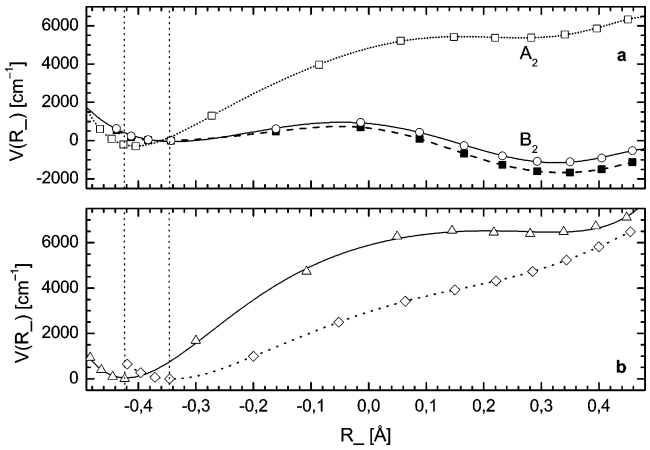

Figure 9. Ab initio H-atom transfer potentials of 1,8-DHAQ. (a) S_2 state (A_2): CIS/6-31G(d,p) (□); S_1 state (B_2): CIS/6-31G(d,p) (○) and TDDFT/6-31G(d,p) energy calculations on the CIS/6−31G(d,p)-MEP geometries (■); (b) S_0 state: HF/6-31G(d,p) (△) and B3LYP/6-31G(d,p) (◇).

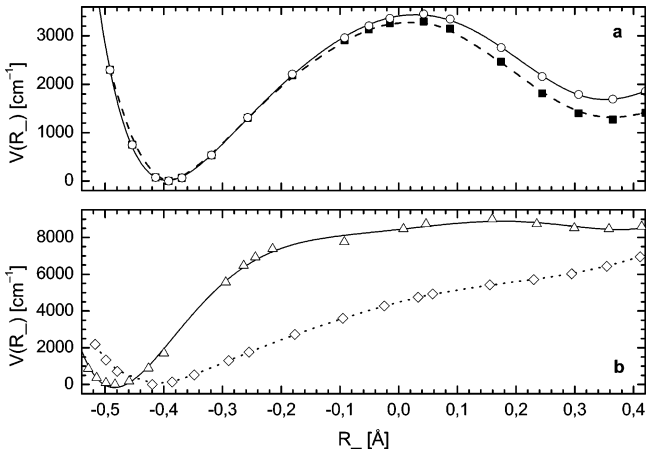

Figure 10. Ab initio H-atom transfer potentials of 1-AAQ. (a) S_1 state: CIS/6-31G(d,p) relaxed PES (○) and TDDFT/6-31G(d,p) energy calculations on the CIS/6-31G(d,p)-MEP geometries (■); (b) S_0 state: HF/6-31G(d,p) (△) and B3LYP/6-31G(d,p) (◇).

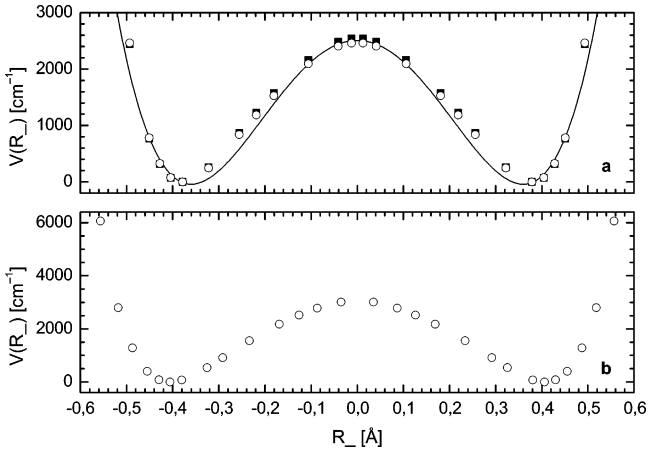

Figure 11. Ab initio H-atom transfer potentials of 9-HPA. (a) S_1 state: CIS/6-31G(d,p) relaxed PES (○) and TDDFT/6-31G(d,p) energy calculations on the CIS/6-31G(d,p)-MEP geometries (■), best-fit model potential according to eq 4 (solid line); (b) S_0 state: HF/6-31G-(d,p) (△).

calculations is to lower the S_1 HT barriers slightly and to stabilize the 1,10-quinone and imine tautomers, respectively. According to the TDDFT calculations, the HT barrier in 1,8-DHAQ is $E_0 \approx 700$ cm^{-1} and the 1,10-quinone tautomer is

stabilized relative to the 9,10-quinone tautomer by ~1700 cm^{-1}. For 1-AAQ, the HT barrier height is $E_0 \approx 3300$ cm^{-1}. In contrast to 1,8-DHAQ, however, the proton-transferred (imine) tautomer is destabilized relative to the amine tautomer by ~1300 cm^{-1}. Particularly noteworthy are the qualitative differences between our ab initio potential energy curves of 1,8-DHAQ and 1-AAQ and the Lippincott−Schroeder potentials,[18,19] which were originally conceived to describe the properties of hydrogen bonds in crystals, but which were subsequently used in the analysis of matrix fluorescence and condensed-phase absorption spectra.[3,6,53] As has been reported previously for the S_0 HT potential energy curve of 1,8-DHAQ calculated on the HF/3-21G level of theory,[5] the ground state does not display a pronounced minimum on the 1,10-quinone side as suggested by the Lippincott−Schroeder potential of Figure 2. Nor do the calculated S_0 HT potential energy curves of 1-AAQ (Figure 10) exhibit such a pronounced minimum. Moreover, the overall topology of the ab initio ground-state potentials relative to the excited-state potentials differs significantly from the corresponding topology of the Lippincott−Schroeder potentials. The excited-state wells of the 1,10-quinone tautomer (1,8-DHAQ) and of the excited-state imine tautomer (1-AAQ) lie almost vertically above the shallow portions of the corresponding S_0 potential energy profiles. It should be noted that the HT coordinate R_- rather is a topological measure (as opposed to a geometrical measure) of the intramolecular hydrogen-bond structure and that a topologically vertical excitation (as opposed to a geometrically vertical excitation) rather corresponds to an adiabatic excitation. However, the overall topological relations between the ground-state and excited-state potential energy curves remain unchanged when the potentials are considered to depend on the simple bond distance R_{O_1H}. Correspondingly, vertical cross-well excitations (Figure 2) into the proton-transferred wells of 1,8-DHAQ and 1-AAQ seem to be rendered very unlikely under supersonic jet conditions.

For 9-HPA, however, the CIS/6-31G(d,p) and TDDFT/6-31G(d,p)//CIS/6-31G(d,p) calculations resulted in almost identical HT potential energy curves (Figure 11). The barrier of the HT process in 9-HPA is ~2500 cm^{-1}. In an effort to assess the appropriateness of one-dimensional HT potential energy profiles calculated on the TDDFT/6-31G(d,p)//CIS/6-31G(d,p) level of theory to describe excited-state tunneling splittings, we calculated the splitting of the vibrational ground state of the S_1 state according to the method of Somorjai and Hornig.[54] For this purpose, a best-fit model potential function to the TDDFT/6-31G(d,p)//CIS/6-31G(d,p) energies of Figure 11 was determined, which consisted of a quadratic and a quartic term

$$V(R_-) = V_2 R_-^2 + V_4 R_-^4 \tag{4}$$

with $V_2 = -3.936 \times 10^4$ $cm^{-1}Å^{-2}$ and $V_4 = 1.520 \times 10^5$ $cm^{-1}Å^{-4}$. The eigenvalues and eigenfunctions of the Schrödinger equation

$$\frac{d^2\Psi(\xi)}{d\xi^2} + \frac{1}{2}(E' - V')\,\Psi(\xi) = 0 \tag{5}$$

were calculated variationally by diagonalization of the $N \times N$ Hamilton matrix, where N denotes the number of basis functions used in setting up the Hamilton matrix. The diagonalization yielded according to

$$\mathbf{C}^{-1}\,\mathbf{H}\,\mathbf{C} = \Lambda \tag{6}$$

the diagonal matrix Λ, which contains the first N energy eigenvalues $E' = 4E/\hbar\beta$, and the coefficient matrix $\mathbf{C}$, whose column vectors contain the expansion coefficients c_{ni} of the first N eigenfunctions $\Phi_i(\xi)$ in the eigenfunction basis $u_n(\xi)$ of the harmonic oscillator. The Hamilton matrix elements are functions of the potential parameters v_2 and v_4 contained in the potential function

$$V(\xi) = \frac{1}{2}\hbar\beta(v_2\xi^2 + v_4\xi^4) \tag{7}$$

and are given explicitly in ref 54. The potential parameters of eq 7 are related to the potential parameters of eq 4 by

$$v_2 = \frac{2V_2}{\mu\beta^2} \quad \text{and} \quad v_4 = \frac{2\hbar V_4}{\mu^2\beta^3} \tag{8}$$

where β is an arbitrary frequency and μ is the reduced mass of the intramolecular hydrogen bond. For simplicity, we assigned μ the value of the proton mass (1.674×10^{-27} kg).

As has been shown previously by Fluder and de la Vega[49] for malonaldehyde, a consideration of the O-atom motions along the MEP increases the reduced mass, μ, by up to more than four times the proton mass. Therefore, taking only the simple proton mass into account is somewhat arbitrary because this assumption corresponds more to a least motion path than to a minimum energy path. Under this assumption and with the potential parameters V_2 and V_4 of eq 4, we calculated a S_1 tunneling splitting of the vibrational ground state of $\Delta_0' = 33$ cm^{-1}. This value deviates strongly from tunneling splittings proposed in previous publications.[20,21] Bondybey and co-workers[21] studied the matrix absorption spectra and the fluorescence dispersion (FD) spectra of several vibronic transitions of 9-HPA and its isotopomer 9-DPA in a neon matrix. On the basis of an analysis of the frequency shifts after deuteration, they determined a S_1 tunneling splitting of the vibrational ground state of $\Delta_0' = 311$ cm^{-1} and a S_0 tunneling splitting of $\Delta_0'' = 69$ cm^{-1}. Rossetti and co-workers[20] studied the FE spectra and the FD spectra of the 0_0^0 transitions of 9-HPA and 9-DPA in neon and argon matrices. From the analysis of a temperature-dependent band at 160 cm^{-1} in the FE spectrum of 9-DPA, which was assigned to the 0_-^- transition, they derived S_0 and S_1 tunneling splittings of the vibrational ground states for 9-HPA of $\Delta_0'' = 127$ cm^{-1} and $\Delta_0' = 617$ cm^{-1}, respectively. Thus, the previously published tunneling splittings are a factor 9−19 higher than ours. A special feature of our calculated S_1 tunneling splitting is that it is a prediction based solely on a one-dimensional ab initio potential energy profile. However, a closer examination of the low-energy transitions of the FE spectrum given in Figure 15 shows that the low-intensity bands at excess energies of −46 and 33 cm^{-1} can be assigned to the parity-allowed 0_-^- and the parity-forbidden 0_+^- transition, respectively. The assignment of the 0_-^- transition is based on the S_0 tunneling splitting of $\Delta_0'' = 69$ cm^{-1} determined in a neon matrix, which is favored in a more recent publication[25] on account of calculations according to the reaction surface Hamiltonian method, which yielded a S_0 tunneling splitting of $\Delta_0'' = 78$ cm^{-1}.

Finally, in an attempt to characterize the topology of the S_0 HT potential energy profile relative to the S_1 HT potential energy profile of 1,8-DHAQ more precisely, we calculated S_0 equilibrium geometries and HT potential energy curves on the HF/6-31G(d,p) as well as on the B3LYP/6-31G(d,p) level of theory. Such a topological characterization was rendered necessary by the close vicinity of two excited states: an excited state of B_2

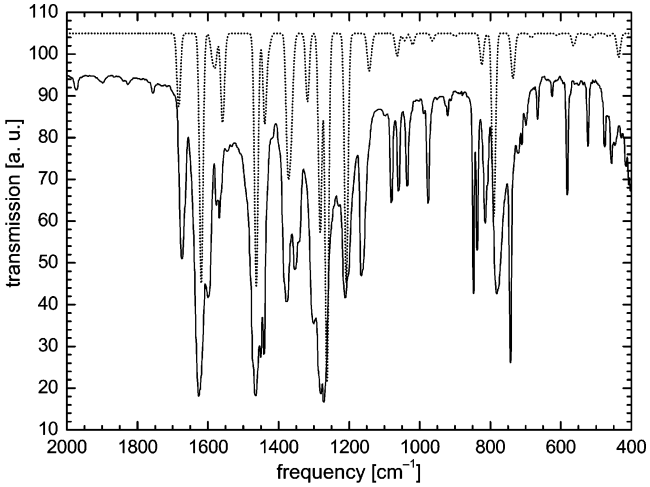

Figure 12. Infrared spectrum from ref 36 (full line) and calculated spectrum (dotted line, B3LYP/6-31G(d,p)) of 1,8-DHAQ. For better visual comparison, the calculated spectrum was convoluted with a Gaussian line shape of fwhm = 5 cm^{-1}.

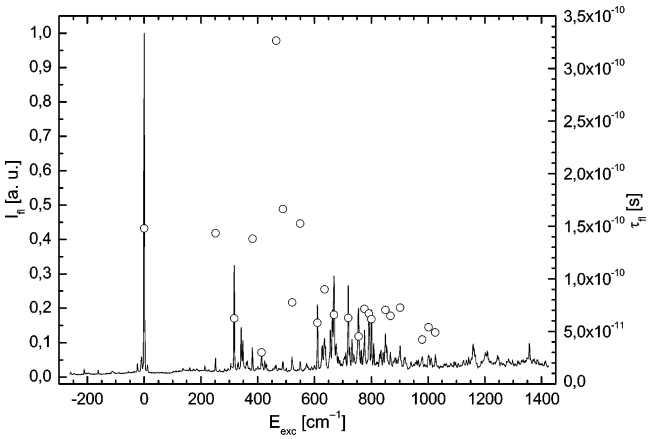

Figure 13. Fluorescence excitation spectrum and estimated major components of the fits to the fluorescence decay curves of 1,8-DHAQ.

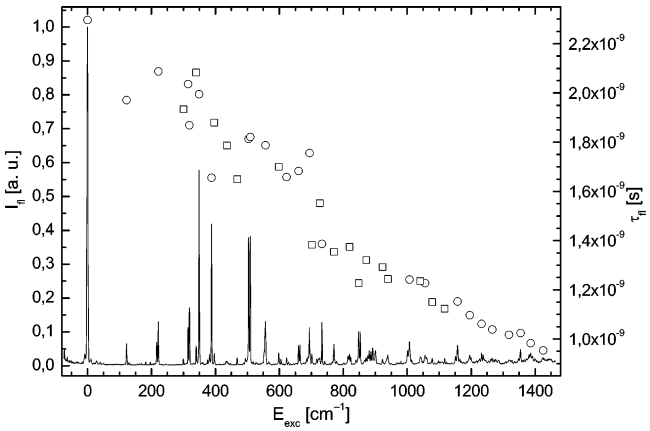

Figure 14. Fluorescence excitation spectrum and fluorescence lifetimes $\bar{\tau}_{fl}$ of 1-AAQ: single-exponential fits (○) and double-exponential fits (□).

orbital symmetry and of predominant LUMO ← HOMO character (S_1) and an excited state of A_2 orbital symmetry and of predominant LUMO ← HOMO−4 character (S_2). As the dotted vertical lines in Figure 9 indicate, the excited state of A_2 symmetry is the lower one upon (topologically) vertical excitation from the HF/6-31G(d,p) equilibrium geometry, whereas the excited state of B_2 symmetry is the lower one upon (topologically) vertical excitation from the B3LYP/6-31G(d,p) equilibrium geometry.

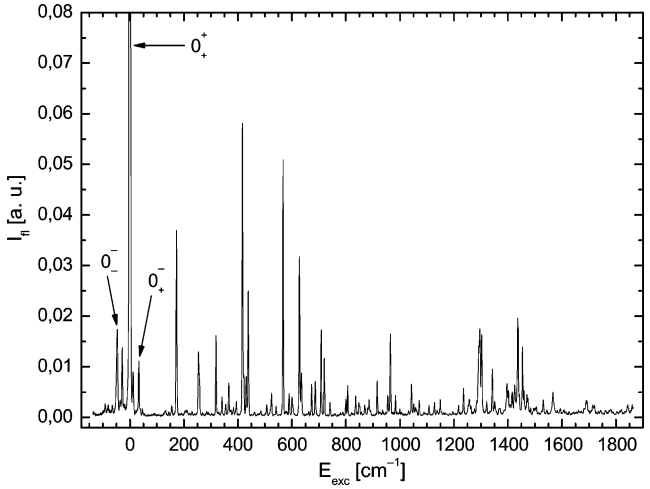

Figure 15. Fluorescence excitation spectrum of 9-HPA.

TABLE 1: Comparison of Crystal Structure Bond Lengths of 1,8-DHAQ and ab Initio Values Calculated on the HF/6-31G(d,p) and B3LYP/6-31G(d,p) Levels of Theory

			bond length (Å)	
bond	exp[a]	exp[b]	HF/6-31G(d,p)	B3LYP/6-31G(d,p)
$C_{18}-O_{22}$	1.357	1.31	1.326	1.338
$C_{18}-C_{19}$	1.397	1.42	1.399	1.408
$C_{19}-C_{21}$	1.371	1.34	1.370	1.386
$C_{20}-C_{21}$	1.371	1.41	1.395	1.402
C_5-C_{20}	1.393	1.40	1.373	1.389
C_5-C_6	1.397	1.39	1.409	1.419
C_6-C_{18}	1.404	1.47	1.401	1.420
C_1-C_6	1.457	1.50	1.474	1.461
C_4-C_5	1.491	1.50	1.495	1.493
C_1-O_7	1.241		1.222	1.266
C_4-O_8	1.224		1.195	1.226
O_7-O_{22}		2.49	2.608	2.570

[a] From ref 28, $R = 0.078$. [b] From ref 34, $R = 0.185$, standard deviation of the bond lengths ±0.04 Å.

Spectroscopic and crystallographic information supporting the appropriateness of either the HF/6-31G(d,p) or the B3LYP/6-31G(d,p) calculation in giving reliable S_0 equilibrium geometries of 1,8-DHAQ is rather sparse. There are, to the best of our knowledge, two X-ray diffraction studies with R factors of $R = 0.18$[34] and $R = 0.078$.[28] In Table 1, we give a comparison between our calculated structural parameters of the S_0 state of 1,8-DHAQ and the corresponding experimental values as given in the X-ray diffraction studies.[28,34] We suggest to prefer the direct comparison with the experimental study of higher quality (second column).[28] Moreover, we decided not to compare our calculated bond angles with their experimental counterparts reported in ref 34 because the experimental error of ∼2° seems to be too large for a conclusive comparison.

In a previous investigation,[5] the HF/3-21G and HF/6-31G(d,p) methods were preferred to the B3LYP/6-31G(d,p) method with regard to the reliability of the calculated HT barrier of 9-HPA and the equilibrium structures of 1,4-DHAQ, 1,5-DHAQ, and 1,8-DHAQ. Our findings, however, cast some doubt on this preference for three reasons. First, the various experimental bond lengths are reproduced differently well on the HF/6-31G(d,p) and B3LYP/6-31G(d,p) level of theory, the B3LYP/6-31G(d,p) method giving a slightly smaller overall deviation from the findings of the higher quality experimental study. Particularly the O_7-O_{22} distance involved in the quasi-conjugate intramo-

lecular H-chelate ring is better reproduced on the B3LYP/6-31G(d,p) level of theory. Our finding of a better overall description of the 1,8-DHAQ geometry with the B3LYP/6-31G(d,p) method is also in line with previous calculations on the naphthazarine geometry with the B3LYP/6-311G(d,p) method.[55] Second, the (topologically) vertical excitation originating in the B3LYP/6-31G(d,p) equilibrium geometry yields the excited state of B_2 symmetry as the first excited electronic state and the excited state of A_2 symmetry as the second excited electronic state. This result is in agreement with the rotational band contour simulation of the most prominent low-energy transition of the FE spectrum given in Section 4.1.1. It should be noted, however, that genuine vertical excitations originating in the B3LYP/6-31G(d,p) as well as in the HF/6-31G(d,p) equilibrium geometries yield the reverse order for the first two excited states (Table X, available as Supporting Information). Third, the comparison of our calculated infrared spectra with the experimental spectrum shows that the HF/6-31G(d,p) spectrum is of much poorer quality than the B3LYP/6-31G(d,p) spectrum that is given in Figure 12 for illustration of its quality. The explicit assignment of the infrared spectrum of 1,8-DHAQ aided by the B3LYP/6-31G(d,p) normal-mode frequencies as well as the infrared spectra of 1-AAQ and 9-HPA and their assignments based on B3LYP/6-31G(d,p) normal-mode frequencies are available as Supporting Information (Figures I and II, Tables VII−IX).

4. Results and Discussion

4.1. Spectroscopy. *4.1.1. Fluorescence Excitation Spectra.* The fluorescence excitation spectra of 1,8-DHAQ, 1-AAQ, and 9-HPA are given in Figures 13, 14, and 15, respectively, relative to their 0_0^0 band origins at $E(0_0^0) = (22089 \pm 2)$ cm^{-1} for 1,8-DHAQ, $E(0_0^0) = (21233 \pm 2)$ cm^{-1} for 1-AAQ, and $E(0_0^0) = (23223 \pm 2)$ cm^{-1} for 9-HPA. Previously reported absolute energies of the 0_0^0 transitions are $E(0_0^0) = 22031$ cm^{-1} for 1,8-DHAQ,[4] $E(0_0^0) = 21183$ cm^{-1} for 1-AAQ,[27] and $E(0_0^0) = 23298$ cm^{-1} for 9-HPA.[25] Obviously, there is a systematic deviation between our absolute energies and those reported previously, ours being 50−76 cm^{-1} ($\triangleq$1.1−1.4 nm) higher in energy. The reason for this deviation, however, is unclear because our interferometric wavelength calibration device (Burleigh, Wavemeter WA-5500) used for daily wavelength calibration has an accuracy of ± 0.2 cm^{-1}. Despite this deviation concerning absolute energies, our FE spectra of 1,8-DHAQ and 1-AAQ show very good agreement with the FE spectra reported previously[4,27] for the identity of the observed vibronic transitions. Moreover, the relative intensities in our FE spectra display good agreement with those from the literature. However, this agreement can be observed only within certain excess energy intervals. For 1,8-DHAQ, the relative intensities agree well within the intervals 0−300 cm^{-1}, 300−600 cm^{-1}, and 600−900 cm^{-1}, separately. A comparison of the relative intensities between these intervals, however, shows that the intensities of the latter section are overestimated by a factor 3−4 in the literature spectrum[4] compared to the relative intensities of our spectrum in the same section. For 1-AAQ, similar relative intensity discrepancies can be found, the agreement being very good within the intervals 0−300 cm^{-1}, 300−500 cm^{-1}, and 500−900 cm^{-1}. Thus, while in our spectra (Figures 13 and 14) the electronic band origins 0_0^0 are the most prominent transitions, the literature spectrum of 1,8-DHAQ[4] has the vibronic transition at 662 cm^{-1} as its most prominent band, the literature spectrum of 1-AAQ[27] the vibronic transition at 501 cm^{-1}. It should be pointed out that these intensity discrepancies certainly cannot be attributed to a difference between laser-power-curve corrected and uncorrected spectra. We corrected all of our fluorescence excitation spectra for the power curves of the dye-laser but noticed only minor intensity differences between the corrected and the uncorrected spectra. The discrepancy could, however, result from the composition of the spectra from different experimental scans. In this respect, the special feature of our spectra of 1,8-DHAQ and 1-AAQ is that they both consist of a single scan.

A further discrepancy between our spectra and those reported in the literature lies in the peculiarity that both literature spectra appear compressed by ~11 cm^{-1} relative to our spectra. This is another systematic deviation for which we cannot conceive an explanation. For 1,8-DHAQ as well as for 1-AAQ, we could extend the excess energy ranges of the corresponding FE spectra (−250−1400 cm^{-1} and −75−1450 cm^{-1}, respectively) as compared to earlier investigations.[4,27]

Our FE spectrum of 9-HPA in a supersonic jet (Figure 15) is, to the best of our knowledge, the first to be reported with a sufficiently high signal-to-noise ratio to be able to distinguish a multitude of vibronic transitions. The FE spectrum of Mori and co-workers reported previously[25] displays a considerably lower signal-to-noise ratio. The difficulty of obtaining a high signal-to-noise ratio with 9-HPA certainly consists in the relative weak intensities of the vibronic transitions as compared to the overwhelming intensity of the band assigned as 0_+^+. As can be seen from the scaling of the ordinate in Figure 15, the most prominent vibronic transition at 417 cm^{-1} has only ~6% of the intensity of the 0_+^+ transition.

In an attempt to assign the vibronic transitions of the FE spectra of all of our model systems, we calculated S_1 normal-mode frequencies on the CIS/6-31G(d,p) (1,8-DHAQ and 9-HPA) and CIS/6-31G(d) (1-AAQ) levels of theory (Tables V and VI, available as Supporting Information). However, we succeeded only to determine a reasonable but tentative assignment for 1-AAQ. The assignment of Table 2 is based on the assumption that 1-AAQ possesses C_s point-group symmetry in both the S_0 and the S_1 state. We, thus, deem the S_0 equilibrium conformation calculated on the B3LYP/6-31G(d,p) level of theory to be preferable to the HF/6-31G(d,p) conformation, which is of C_1 point-group symmetry. With 1-AAQ possessing C_s point-group symmetry in both electronic states, the 72 vibrational modes factorize into two symmetry species: 49 totally symmetric a' modes ($\nu_1-\nu_{49}$) and 23 nontotally symmetric a'' modes ($\nu_{50}-\nu_{72}$). According to the pertinent electric dipole selection rules, all fundamental, overtone, and combination bands are allowed for the a' modes, whereas for the a'' modes only those overtone and combination bands with an even number of quanta are predicted to have nonvanishing intensities.[45] From the assignment of Table 2, the S_1 frequencies of 27 normal modes could be determined (Table 3). The experimental values tabulated for the a'' normal modes were calculated from their first overtones by dividing the observed frequency values by two. According to our assignment, the spectrum contains only few progressions and combination bands as is expected for an electronic transition upon which there are only slight conformational changes. The only overtone progressions worth mentioning are those of the normal modes ν_{45} and ν_{46}. The former normal mode corresponds predominantly to an in-plane symmetric wagging motion of the carbonyl O atoms, the latter is an in-plane C-skeleton deformation, both normal modes giving rise to strong deformations of the intramolecular H-chelate ring.

Interestingly, we could not confirm a previously advanced conjecture[28] that the splitting by ~5 cm^{-1} of several prominent

TABLE 2: Assignment for the S_1 Fluorescence Excitation Frequencies (cm^{-1}) of 1-AAQ Relative to the 0_0^0 Band Origin at (21233 ± 2) cm^{-1}, Whose Intensity Was Arbitrarily Set to 100[a]

ν_{FES}	I_{FES}	assignment	remarks
0	100	0_0^0	
122	7	71_0^2	
216	7	49_0^1	D
221	13	70_0^2	D
300	2	69_0^2	
315	11	48_0^1D	
319	17	47_0^1	D
340	6	68_0^2	
349	58	46_0^1	
388	42	45_0^1	
468	2	43_0^1	
504	38	67_0^2	D
509	38	$45_0^1 71_0^2$	D
557	13	42_0^1	
598	4	41_0^1	
623	2	48_0^2	
660	6	40_0^1, $46_0^1 48_0^1$	D
664	6	39_0^1, $46_0^1 47_0^1$	D
694	11	46_0^2	
734	13	38_0^1, 66_0^2, $45_0^1 46_0^1$	
771	6	45_0^2	
815	3	$41_0^1 49_0^1$	FR
820	3	$41_0^1 70_0^2$, $48_0^1 66_0^2$	FR
823	3	$47_0^1 67_0^2$, $45_0^1 48_0^1 71_0^2$	FR
848	10	65_0^2, $46_0^1 67_0^2$	D
853	10	37_0^1, $38_0^1 71_0^2$, $66_0^2 71_0^2$, $45_0^1 46_0^1 71_0^2$	D
881	4	$45_0^1 67_0^2$	FR
887	4	$45_0^2 71_0^2$	FR
891	5	36_0^1	FR
901	4	64_0^2, $42_0^1 46_0^1$	FR
940	3	63_0^2	
1007	7	34_0^1	
1041	3	46_0^3	
1056	3	32_0^1, $45_0^1 46_0^1 47_0^1$	
1078	2	$45_0^1 46_0^2$	
1117	2	$38_0^1 45_0^1$, $45_0^2 46_0^1$, $45_0^1 66_0^2$	
1151	3	45_0^3	D
1158	6	27_0^1	D
1195	3	41_0^2, $46_0^2 67_0^2$	
1233	4	25_0^1	
1354	5	22_0^1	

[a] FR denotes components of multiple Fermi resonances, D the components of doublets.

features of the FE spectrum of 1-AAQ (marked with D for doublet in Table 2) is due to the coupling between normal modes involving the intramolecular hydrogen bond and a normal mode representing N-inversion through the molecular plane with frequencies of 118 cm^{-1} in the S_1 state and 80 cm^{-1} in the S_0 state.[27] In the S_0 state, five normal modes (ν_{71}, ν_{70}, ν_{69}, ν_{68}, and ν_{67}) exhibit considerable inversion-type character, ν_{67} (225 cm^{-1}) resembling most a pure inversion without contributions from C-skeleton or H-atom out-of-plane motions. In the S_1 state, however, strong Duschinsky rotation[56] distributes the inversion-type motional character over 11 normal modes (ν_{67}, ν_{66}, ν_{64}, ν_{63}, ν_{62}, ν_{60}, ν_{59}, ν_{58}, ν_{57}, ν_{56}, and ν_{55}), the normal modes ν_{62} (522 cm^{-1}) and ν_{55} (793 cm^{-1}) presumably having the strongest inversion-type character. Our finding of strong Duschinsky rotation based on our CIS normal mode calculations is in line with previous results based on an analysis of the fluorescence dispersion spectra of several vibronic transitions.[27] A comparison with the assignment of Table 2 shows that only normal mode ν_{67} could account for merely two doublets. We feel, however, that these splittings, particularly for their uniform value of ~5 cm^{-1}, might be of generic character for 1-AAQ and should, therefore, receive a generic analysis. For this reason, we prefer to regard our assignment of Tables 2 and 3 as tentative. Furthermore, the transition at 122 cm^{-1} in our FE spectrum and at 118, cm^{-1} in the previously reported jet spectrum,[27] which is missing in the corresponding matrix spectrum,[26] is assigned to the first overtone of the S_1 normal mode ν_{71}. This normal mode corresponds to a twist (torsion) of the phenyl ring carrying the amine group around the rest of the molecule. We, thus, confirm and make more precise the previously advanced conjecture[27] that this band could be due to a puckering motion of the six-membered H-chelate ring and might be dampened in the matrix environment.

TABLE 3: Experimental Frequencies ν_{FES} of the Fluorescence Excitation Spectrum of 1-AAQ and Frequencies ν_{calcd} Calculated on the CIS/6-31G(d) Level of Theory

ν_{FES} (cm^{-1})	ν_{calcd} (cm^{-1})	$\Gamma_j^{(1)}(l_i')$	S_1 normal mode
61.1	56.2	a''	ν_{71}
111	129	a''	ν_{70}
150	153	a''	ν_{69}
170	185	a''	ν_{68}
216	212	a'	ν_{49}
252	237	a''	ν_{67}
315	312	a'	ν_{48}
319	329	a'	ν_{47}
349	368	a'	ν_{46}
367	371	a''	ν_{66}
388	399	a'	ν_{45}
424	419	a''	ν_{65}
450	452	a''	ν_{64}
468	471	a'	ν_{43}
470	482	a''	ν_{63}
557	530	a'	ν_{42}
598	573	a'	ν_{41}
660	638	a'	ν_{40}
664	667	a'	ν_{39}
734	754	a'	ν_{38}
853	837	a'	ν_{37}
891	880	a'	ν_{36}
1007	1011	a'	ν_{34}
1056	1078	a'	ν_{32}
1158	1162	a'	ν_{27}
1233	1222	a'	ν_{25}
1354	1358	a'	ν_{22}

As has been noted previously by Fernández-Ramos and coworkers,[23] S_1 normal-mode frequencies calculated on the CIS/6-31G(d,p) level of theory are not appropriate for an assignment of the matrix FE spectra of 9-HPA.[20−22] They attributed this failure to a complication of the spectrum due to the interaction with nearby excited states. To check this assumption more quantitatively, we calculated vertical excitation energies on the CIS/6-31G(d,p) level of theory with the HF/6-31G(d,p) equilibrium geometry. Table 4 shows that only triplet states, among them especially T_5, are energetically close to the first excited singlet state S_1. This finding would also accommodate for the observation of phosphorescence in matrix studies.[21,22] In agreement with previous results[51] however, the CIS method yields much to high vertical excitation energies.

As in the case of 9-HPA, an assignment of the FE spectrum of 1,8-DHAQ with S_1 normal-mode frequencies calculated on the CIS/6-31G(d,p) level of theory turned out to be unfeasible.

TABLE 4: Symmetry Species and Vertical Excitation Energies VE_{calcd} of the Lowest Triplet and Singlet Excited Electronic States of 9-HPA Calculated at the CIS/6-31G(d,p) Level of Theory with the HF/6-31G(d,p) Equilibrium Geometry

state	symmetry	VE_{calcd} (eV)	VE_{exp} (eV)
S_0	$\tilde{X}\ ^1A_1$		
T_1	$\tilde{a}\ ^3A'$	2.48	
T_2	$\tilde{b}\ ^3A'$	3.41	
T_3	$\tilde{c}\ ^3A'$	3.62	
T_4	$\tilde{d}\ ^3A'$	4.23	
S_1	$\tilde{A}\ ^1A'$	4.60	2.88
T_5	$\tilde{e}\ ^3A'$	4.66	
T_6	$\tilde{f}\ ^3A''$	4.73	
T_7	$\tilde{g}\ ^3A'$	5.04	
S_2	$\tilde{B}\ ^1A'$	5.14	
S_3	$\tilde{C}\ ^1A''$	5.25	
T_8	$\tilde{h}\ ^3A'$	5.57	
S_4	$\tilde{D}\ ^1A'$	5.62	

We attribute this failure to the close proximity of S_1 and S_2 states and the occurrence of an intersection between them close to the Franck−Condon region as illustrated in Figure 9. Furthermore, we agree with previous analyses[3,4] to interpret the FE spectrum of Figure 13 as consisting of two distinct excess energy regions. On the basis of our ab initio calculations, we, however, propose that the first region from 0 to 600 cm^{-1} contains Franck−Condon-allowed transitions terminating in the excited state of B_2 symmetry, whose fluorescence is quenched predominantly by the nearby intersection with the excited state of A_2 symmetry. The bands of the second region from ∼600 cm^{-1} upward are of comparatively high intensity and derive from transitions originating not only in vibrational levels of the 9,10-quinone well but also in levels of the 1,10-quinone well, which becomes accessible above the HT barrier (Figure 9). In an attempt to obtain conclusive evidence of the correct relative topology between the S_0 state on one hand and the S_1 and S_2 state on the other hand, we carried out a rotational band contour simulation of the vibrationless electronic transition 0_0^0 given in ref 4. Figure 16 shows the experimental band contour of ref 4 together with a fit obtained with the freeware program PGOPHER.[57] Fit parameters were the rotational constants of the S_0 and S_1 states (B_2), the rotational temperature, T_{rot}, and the full widths at half-maxima (fwhm) of a Gaussian and a Lorentzian line profile giving together a Voigt line profile. The best fit was obtained by varying manually single parameters

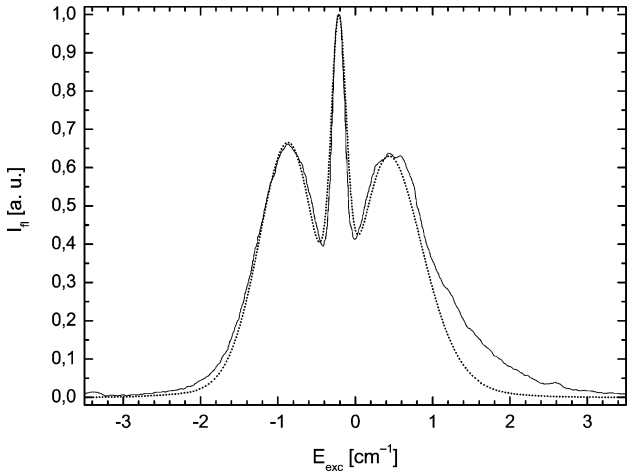

Figure 16. Rotational band contour of the 0_0^0 transition of the FE spectrum of 1,8-DHAQ taken from ref 4 (full line) and rotational band contour simulation (dotted line). The rotational temperature is T_{rot} = 19 K.

TABLE 5: Fit Parameters of the Rotational Band Contour Simulations of 1,8-DHAQ[a]

	ground state			excited state					
	A	B	C	A	B	C	T_{rot} (K)	$\Delta\tilde{\nu}_{Gauss}$	$\Delta\tilde{\nu}_{Lorentz}$
Set 1	763.9	376.1	252.0	764.2	376.8	252.5	19	0.18	0.12
Set 2	748.6	374.7	249.7	749.5	373.2	251.2	20	0.18	0.12

[a] Set 1 contains the unchanged S_0 rotational constants calculated on the HF/6-31G(d,p) level of theory; set 2 contains the rotational constants calculated on the B3LYP/6-31G(d,p) level of theory. The CIS/6-31G(d,p) rotational constants of the S_1 state are the following: A = 765.6 MHz, B = 376.8 MHz, and C = 252.5 MHz. All rotational constants are given in MHz; $\Delta\tilde{\nu}_{Gauss}$ and $\Delta\tilde{\nu}_{Lorentz}$ are in cm^{-1}. The temporal laser pulse width is reported[4] to be 0.002 nm ($\hat{\approx}$0.1 cm^{-1}).

while assessing visually every change of the P−R-branch separation, the P−R-branch intensity ratio and the relative Q-branch intensity. Selection rules appropriate for long-axis (parallel) polarization of the $S_1 \leftarrow S_0$ transition dipole moment were assumed, and rotational quantum numbers up to J = 150 were taken into account. For the rotational contour simulation of Figure 16, the set of parameters denoted as Set 1 in Table 5 were used. Set 2 gave a rotational contour of similar quality, the differences between the rotational constants of both sets, thus giving estimates for the uncertainties of the rotational constants. Set 1 contains the S_0 rotational constants calculated on the HF/6-31G(d,p) level of theory, whereas Set 2 contains the rotational constants calculated on the B3LYP/6-31G(d,p) level of theory. For a satisfactory fit, all S_1 rotational constants had to be changed from their values calculated on the CIS/6-31G(d,p) level of theory in the case of Set 2, whereas with Set 1 only the S_1 rotational constant A had to be changed from its calculated value. We, therefore, feel reluctant to decide on account of the rotational contour simulation whether the HF/6-31G(d,p) or the B3LYP/6-31G(d,p) calculation describes the S_0 equilibrium conformation of 1,8-DHAQ more appropriately. However, it should be clear from Figure 16 that, even though our fit is not perfect, the agreement in overall shape indicates that the most prominent low-energy transition is predominantly parallel polarized and, consequently, terminating in the excited state of B_2 symmetry. The rotational band contour simulation, thus, supports our assumption that the first excited-state possesses B_2 orbital symmetry and gives rise to Franck−Condon-allowed, parallel polarized transitions.

Moreover, previous findings of Gillispie and co-workers[4] show that most of the rotational band contours change fundamentally in shape for excess energies above ∼600 cm^{-1}. Although the rotational band contours below ∼600 cm^{-1} are of the type given in Figure 16, most of the rotational contours above ∼600 cm^{-1} lack the dominating Q-branch and are, therefore, certainly not parallel polarized. We interpret this finding as support in favor of our previous assumptions[3,4] that these bands are due to transitions originating in the 1,10-quinone well. The difference between our point of view and the previously advanced conjectures is that the fluorescence originating in the 1,10-quinone well is not preceded by vertical cross-well absorption into this well, but by vertical absorption into the 9,10-quinone well and subsequent fast ESIPT above the HT barrier, which should rather be compared to fast intramolecular vibrational relaxation. We, thus, favor case c of ref 4. The HT barrier of ∼700 cm calculated on the TDDFT/6-31G(d,p)//CIS/6-31G(d,p) level of theory (Figure 9) supports our assumption as well as the time-resolved fluorescence measurements presented in the next section.

4.2. Dynamics. *4.2.1. Fluorescence Lifetimes.* The fluorescence lifetimes $\tau_{fl}(E)$ of a multitude of vibronic transitions of

jet-cooled isolated 1,8-DHAQ (Figure 13), 1-AAQ (Figure 14) and 9-HPA (not given in Figure 15) were determined by time-correlated single photon counting[41] as a function of excess vibrational energy. The fluorescence decay curves were analyzed by a least-squares convolution and fitting routine using the Levenberg−Marquardt algorithm.[58,59]

The fluorescence decay curves of 1,8-DHAQ turned out to be highly nonexponential. Not even triple-exponential fits yielded satisfactory results for the entire time range of 2048 channels. Notwithstanding, double-exponential fits over a small range of the fluorescence decay curves at early delay times (300 channels), which were still of poor quality, served to determine estimates for the fluorescence lifetimes. All fit parameters of the fluorescence decay curves of 1,8-DHAQ are available as Supporting Information (Table I). The major component τ_1 of the double-exponential fits, whose relative amplitude was >97% in every case, is given in Figure 13. As can be seen from the scaling of the right ordinate of Figure 13, all estimated fluorescence lifetimes, lying in the range between 30 and 330 ps, are very close to the fwhms of our instrument response functions (50−70 ps). This finding provides an additional caveat, suggesting to conceive the major component τ_1 merely as an estimate of the falloff time of the corresponding fluorescence decay curve. With these provisos in mind, we, nonetheless, think that the estimated fluorescence lifetimes of Figure 13 support our assumption of a two-region-type FE spectrum and, moreover, our conjecture that the vibronic bands above ∼600 cm^{-1} are due to a different tautomer. We draw this conclusion from the observation that below ∼600 cm^{-1} the estimated fluorescence lifetimes show a strong scatter around ∼150 ps, whereas above ∼600 cm^{-1} they exhibit a smaller scatter around ∼60 ps.

Although the estimated lifetimes of 1,8-DHAQ show no uniform excess energy dependence, such a monotonic energy dependence, superposed by a moderate state-selective scatter, can be observed in the case of 1-AAQ (Figure 14). Furthermore, the mean fluorescence lifetimes of 1-AAQ are much longer than those of 1,8-DHAQ and lie between ∼2.3 ns for the vibrationless 0_0^0 transition and ∼950 ps for the vibronic transition at 1425 cm^{-1}. All of the fluorescence decay curves of 1-AAQ could be fitted satisfactorily over the entire time range by either single-exponential or double-exponential model functions. As an example, in Figure 17, the fluorescence decay curve at $E_{exc} = 940$ cm^{-1} is given together with a double-exponential fit. The residuals and their autocorrelation function (ACF) illustrate the high quality of the fit. We could quantitatively account for the uniform excess energy dependence of the fluorescence lifetimes in a quite satisfactory way using Fermi's Golden Rule[37,38]

$$\frac{1}{\tau_{fl}(E)} = k_{fl}(E) = k_{rad} + \frac{2\pi}{\hbar}|V_{if}|^2 \rho_{S_0}(E) = k_{rad} + c\cdot\rho_{S_0}(E) \tag{9}$$

For the calculation of the density of states $\rho_{S_0}(E)$ in the S_0 state, normal-mode frequencies calculated on the B3LYP/6-31G(d,p) level of theory were used (Table IV, available as Supporting Information). The rate constant k_{rad} of the radiative process and the constant c, containing the modulus $|V_{if}|$ of the mean coupling matrix element between the initial vibronic state i and the final vibronic state f, served as fit parameters. The automatic least-squares fit to the experimental rate constants of fluorescence $k_{fl}(E)$, which yielded values of $k_{rad} = 4.9 \times 10^8$ s^{-1} and $c = 7.9 \times 10^{-17}$ cm^{-1}/s, is given in Figure 18. On the basis of the success of this quantitative account, we attribute the uniform excess energy dependence of the fluorescence lifetimes of 1-AAQ to be due to internal conversion $S_0 \leftarrow S_1$. From our point of view, the absence of any strong coupling to a nearby excited singlet or triplet state and the comparatively weak intramolecular hydrogen bond as reflected by the low charge density at the bond critical point $\rho(\mathbf{r}_c)$ in the S_0 state (Figure 7) and the high HT barrier in the S_1 state (Figure 10) provide reasonable explanations for the relatively long fluorescence lifetimes and their uniformm excess energy dependence.

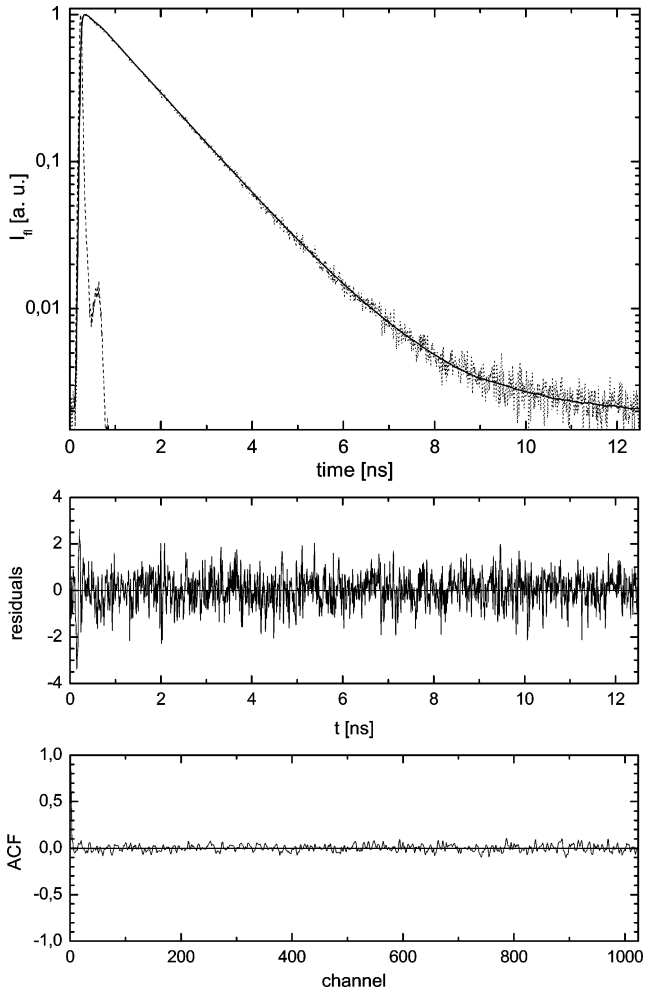

Figure 17. Fluorescence decay curve at $E_{exc} = 940$ cm^{-1} with double exponential fit ($\bar{\tau}_{fl} = 1.243$ ns).

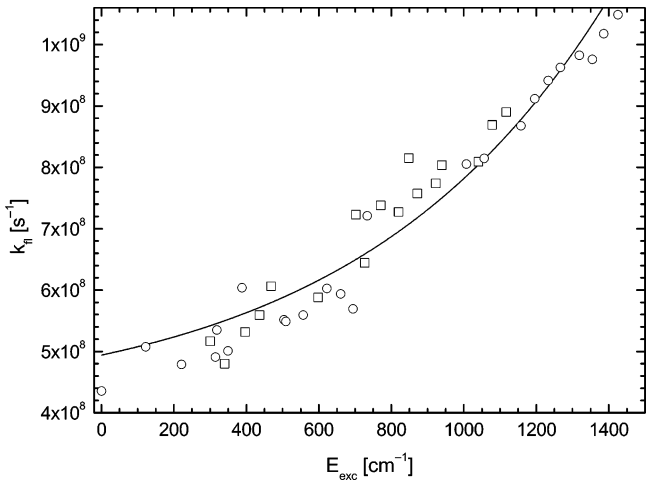

Figure 18. Excess energy dependence of the rate constant k_{fl} of fluorescence and fit according to Fermi's Golden Rule.

For 9-HPA, we have determined estimates for the fluorescence lifetimes of only two transitions: the 0_+^+ transition (~155 ps) and the vibronic transition at 628 cm^{-1} (~56 ps). These fluorescence decay curves exhibited features that obstructed a precise determination of the fluorescence lifetimes and that have already been discussed in the case of 1,8-DHAQ. They were highly nonnonexponential and possessed falloff times close to the time resolution of our TCSPC apparatus (50−70 ps). We, therefore, decided not to determine further fluorescence decays, as in the case of 9-HPA there seemed to be no prospect to reveal fluorescence from a second tautomer as in the case of 1,8-DHAQ. Having calculated only the vertical excitation energies of the lowest triplet and singlet states on the CIS/6-31G(d,p) level of theory 4, we can only speculate about the reasons for the observed very fast fluorescence decays. As we have already noted in Section 4.1.1, only triplet states, particularly T_5, are energetically close to the first excited singlet state S_1. We, therefore, suggest that an intersystem crossing, most probably $T_5 \leftarrow S_1$, is very likely to be the reason for the observed fast fluorescence decays. This assumption would also accommodate for previous findings of structured phosphorescence in matrix luminescence studies.[21,22] We should note that our assumption departs from a previous proposal advanced by Sobolewski and Domcke[52,60] concerning the mechanism of rapid nonradiative decay in an intramolecularly hydrogen-bonded analogue of 9-HPA, malonaldehyde. According to their analysis based on CASPT2 ab initio calculations, the fast nonradiative relaxation of malonaldehyde is associated with a low-lying intersection of the $^1\pi\pi^*$ state with $^1\pi\sigma^*$ and $^1n\sigma^*$ states, which are strongly repulsive with respect to the in-plane, C_{2v} symmetric detachment of the H atom away from both O atoms. The potential energy profile resulting from this intersection would subsequently lead to another low-lying intersection with the S_0 state, thus giving rise to efficient internal conversion to the ground state. Future theoretical efforts should address whether this mechanism, intersystem crossing, or a combined mechanism involving intersections between singlet and triplet states is appropriate for a description of the fast nonradiative fluorescence decays of 9-HPA.

5. Conclusions

The main goal of our present investigation was to determine the influence of structural and energetic features associated with intramolecular hydrogen bonding on the energy- and time-resolved fluorescence properties of large organic molecules. Particularly, we were interested in spectroscopic evidence indicating the occurrence of excited-state intramolecular proton transfer and in the types of potentials (single-minimum type or double-minimum-type) governing the intramolecular hydrogen bonding and the ESIPT processes.

In line with these goals, we carried out energy- and time-resolved fluorescence measurements as well as ab initio calculations on S_0 and S_1 properties of three intramolecularly hydrogen-bonded model systems: 1,8-dihydroxyanthraquinone (1,8-DHAQ), 1-aminoanthraquinone (1-AAQ), and 9-hydroxyphenalenone (9-HPA).

The FE spectra of all three molecules were determined. A comparison with spectra reported previously showed very good agreement for the identity and the relative intensities of the vibronic transitions. However, a conventional normal-mode analysis based on ab initio harmonic normal modes frequencies calculated on the CIS/6-31G(d) level of theory was only feasible for the FE spectrum of 1-AAQ, the tentative assignment giving no evidence for large anharmonicities. We, therefore, favor the assumption that in the excess energy range under investigation (0−1450 cm^{-1}) the energy- and time-resolved fluorescence properties of 1-AAQ are associated with a single-minimum-type potential. This assumption is in line with the occurrence of a uniform excess energy dependence of comparatively long fluorescence liftetimes, which can be quantitatively accounted for according to Fermi's Golden Rule. The success of this analysis indicates that this energy dependence is due to internal conversion into the S_1 state. Thus, there is no indication of the presence of any strong coupling to or intersection with a nearby excited-state destroying the single-minimum-type potential. Further evidence in favor of our assumption is provided by our ab initio calculations. The low charge density at the bond critical point $\rho(\mathbf{r}_c)$ in the S_0 state and the high HT barrier in the S_1 state provide strong indications of the weakness of the intramolecular hydrogen bond in 1-AAQ and of the presence of a single-minimum-type potential in the excess energy range under investigation.

The FE spectrum of 1,8-DHAQ exhibits two distinct excess energy ranges, which were characterized by different spectral congestions and relative intensities in the frequency-domain measurements and by different fluorescence lifetimes in the time-domain measurements. This finding is supported by previously reported[4] rotational band contours of several transitions studied in a supersonic jet. The rotational contour simulation of the most prominent low-energy band showed that this transition is (predominantly) parallel polarized and, hence, terminates in the excited state of B_2 symmetry. All rotational band contours below ~600 cm^{-1} were previously shown to be of this type, whereas most of the rotational band contours above ~600 cm^{-1} lack the dominating Q branch and are, therefore, certainly not parallel polarized. We interpreted these results as support in favor of our previous assumptions[3,4] that the fluorescence bands below ~600 cm^{-1} are due to transitions originating in the 9,10-quinone well, whereas the bands above ~600 cm^{-1} are due to transitions originating in the proton-transferred 1,10-quinone well of the S_1 HT potential. We attracted attention to the difference between our point of view and previously advanced conjectures: The fluorescence originating in the 1,10-quinone well is not preceded by vertical cross-well absorption into this well, but by vertical absorption into the 9,10-quinone well and subsequent fast ESIPT above the HT barrier. This assumption is supported by the value of the S_1 HT barrier of ~700 cm calculated on the TDDFT/6-31G(d,p)//CIS/6-31G(d,p) level of theory. A conventional normal-mode analysis with harmonic frequencies calculated on the CIS/6-31G(d,p) level of theory could not be carried out, this failure being attributed to the nearby intersection of the S_1 state (B_2) with the S_2 state (A_2) and the occurrence of a low S_1 HT barrier. Future theoretical efforts should address our assumption that the ESIPT process gives rise to sufficiently severe changes of the rotational constants corresponding to the 1,10-quinone wells in order to furnish substantially different rotational band contours.

For 9-HPA, only frequency-domain measurements yielded tentative evidence for the presence of a pronounced double-minimum-type potential along the HT path. On the basis of our S_1 HT potential energy curve calculated on the TDDFT/6-31G(d,p)//CIS/6-31G(d,p) level of theory, we calculated the tunneling splitting of the vibrationless level in the S_1 state, which allowed us to assign the bands at −46 and 33 cm^{-1} as the 0_-^- and the 0_+^- transition, respectively. Only two fluorescence lifetimes were estimated from decay curves deriving from fluorescence of the vibrationless transition (~155 ps) and from

the vibronic transition at 628 cm^{-1} (~56 ps). These decay curves turned out to be highly nonexponential and possess falloff times close to the time resolution of our TCSPC apparatus (50−70 ps). We attributed the underlying rapid nonradiative relaxation mechanism to intersystem crossing to a triplet state, most probably $T_5 \leftarrow S_1$. This conjecture is supported by previous observations of phosphorescence in matrix luminescence studies.[21,22]

From a methodological point of view, we think to have provided helpful indications particularly of the prospects of time-resolved fluorescence studies in a supersonic jet in elucidating the occurrence of excited-state intramolecular proton transfer in intramolecularly hydrogen-bonded molecules.

Acknowledgment. Financial support by the Deutsche Forschungsgemeinschaft (Sonderforschungsbereich 357: Molekulare Mechanismen Unimolekularer Prozesse) is gratefully acknowledged.

Supporting Information Available: Detailed information (10 Tables and 2 Figures) about the experimental findings and the ab initio calculations reported in our paper. Here we report the fit parameters of the fluorescence decay curves of 1,8-DHAQ and 1-AAQ, the fluorescence lifetimes of 1-AAQ, the S_0 normal-mode frequencies of all model systems, the S_1 normal-mode frequencies of 1-AAQ and 9-HPA, the S_1 and S_2 normal-mode frequencies of 1,8-DHAQ, the experimental and calculated infrared spectra of 1-AAQ and 9-HPA, the assignments of the infrared spectra of all model systems, and calculated vertical excitation energies of excited singlet and triplet states of 1,8-DHAQ. This material is available free of charge via the Internet at http://pubs.acs.org.

References and Notes

(1) Smulevich, G. *J. Chem. Phys.* **1985**, *82*, 14.
(2) Smulevich, G.; Marzocchi, M. P. *Chem. Phys.* **1986**, *105*, 159.
(3) Smulevich, G.; Foggi, P.; Feis, A.; Marzocchi, M. P. *J. Chem. Phys.* **1987**, *87*, 5664.
(4) Gillispie, G. D.; Balakrishnan, N.; Vangsness, M. *Chem. Phys.* **1989**, *136*, 259.
(5) Ferreiro, M. L.; Rodríguez-Otero, J. *J. Mol. Struct.* **2001**, *542*, 63.
(6) Marzocchi, M. P.; Mantini, A. R.; Casu, M.; Smulevich, G. *J. Chem. Phys.* **1998**, *108*, 534.
(7) Waring, M. J. *Annu. Rev. Biochem.* **1981**, *50*, 159.
(8) Lown, J. W. *Anthracycline and Anthracenedione-Based Anticancer Agents*; Elsevier: Amsterdam, 1988.
(9) Eriksson, M.; Nórden, B.; Eriksson, S. *Biochemistry* **1988**, *27*, 8144.
(10) Nonaka, Y.; Tsuboi, M.; Nakamoto, K. *J. Raman Spectrosc.* **1990**, *21*, 133.
(11) Lown, J. W. *Chem. Soc. Rev.* **1993**, *22*, 165.
(12) Chaires, J. B. *Curr. Opin. Struct. Biol.* **1998**, *8*, 314.
(13) Rabbani, A.; Finn, R. M.; Ausió, J. *BioEssays* **2005**, *27*, 50.
(14) Falk, H. *Angew. Chem.* **1999**, *111*, 3306.
(15) Carpenter, S.; Fehr, M. J.; Petrich, J. W. *Proc. Natl. Acad. Sci. U.S.A.* **1994**, *91*, 12273.
(16) Fehr, M. J.; McCloskey, M. A.; Petrich, J. W. *J. Am. Chem. Soc.* **1995**, *117*, 1833.
(17) Sureau, F.; Miskovsky, P.; Chinsky, L.; Turpin, P. Y. *J. Am. Chem. Soc.* **1996**, *118*, 9484.
(18) Lippincott, E. R.; Schroeder, R. *J. Chem. Phys.* **1955**, *23*, 1099.
(19) Schroeder, R.; Lippincott, E. R. *J. Phys. Chem.* **1957**, *61*, 921.
(20) Rossetti, R.; Haddon, R. C.; Brus, L. E. *J. Am. Chem. Soc.* **1980**, *102*, 6913.
(21) Bondybey, V. E.; Haddon, R. C.; English, J. H. *J. Chem. Phys.* **1984**, *80*, 5432.
(22) Gillispie, G. D. *J. Chem. Phys.* **1986**, *85*, 4825.
(23) Fernández-Ramos, A.; Smedarchina, Z.; Zgierski, M. Z.; Siebrand, W. *J. Chem. Phys.* **1998**, *109*, 1004.
(24) Kovács, A.; Izvekov, V.; Zauer, K.; Ohta, K. *J. Phys. Chem. A* **2001**, *105*, 5000.
(25) Mori, H.; Furusawa, J.; Sekiya, H. *Bull. Pol. Acad. Sci.* **2002**, *50*, 451.
(26) Carter, T. P.; Van Benthem, M. H.; Gillispie, G. D. *J. Phys. Chem.* **1983**, *87*, 1891.
(27) Balakrishnan, N.; Gillispie, G. D. *J. Phys. Chem.* **1989**, *93*, 2337.
(28) Marasinghe, P. A. B.; Gillispie, G. D. *Chem. Phys.* **1989**, *136*, 249.
(29) Bader, R. F. W. *Atoms in Molecules. A Quantum Theory*; Clarendon Press: Oxford, 1990.
(30) Boyd, R. J.; Choi, S. C. *Chem. Phys. Lett.* **1985**, *120*, 80.
(31) Boyd, R. J.; Choi, S. C. *Chem. Phys. Lett.* **1986**, *129*, 62.
(32) Carroll, M. T.; Bader, R. F. W. *Mol. Phys.* **1988**, *65*, 695.
(33) Koch, U.; Popelier, P. L. A. *J. Phys. Chem.* **1995**, *99*, 9747.
(34) Prakash, A. *Z. Kristallogr.* **1965**, *122*, 272.
(35) Ogawa, K.; Kobayashi, H. *Sci. Rep., Osaka Univ.* **1968**, *17*, 15.
(36) Pouchert, C. J. *The Aldrich Library of FT-IR-Spectra*; Aldrich Chemical Co.: New York, 1985; Vol. 2.
(37) Englman, R.; Jortner, J. *Mol. Phys.* **1970**, *18*, 145.
(38) Schatz, G. C.; Ratner, M. A. *Quantum Mechanics in Chemistry*; Prentice Hall: Englewood Cliffs, NJ, 1993.
(39) Müller, C. Ph.D. Thesis, Georg-August-Universität Göttingen, 2005 (available at: http://webdoc.sub.gwdg.de/diss/2005/mueller_christian/mueller_christian.pdf).
(40) Runge, P. K.; Rosenberg, R. *IEEE J. Quantum Electron.* **1972**, *QE-8*, 910.
(41) O'Connor, D. V.; Phillips, D. *Time-Correlated Single Photon Counting*; Academic Press: London, 1984.
(42) Frisch, M. J.; Trucks, G. W.; Schlegel, H. B.; Scuseria, G. E.; Robb, M. A.; Cheeseman, J. R.; Zakrzewski, V. G.; Montgomery, J. A., Jr.; Stratmann, R. E.; Burant, J. C.; Dapprich, S.; Millam, J. M.; Daniels, A. D.; Kudin, K. N.; Strain, M. C.; Farkas, O.; Tomasi, J.; Barone, V.; Cossi, M.; Cammi, R.; Mennucci, B.; Pomelli, C.; Adamo, C.; Clifford, S.; Ochterski, J.; Petersson, G. A.; Ayala, P. Y.; Cui, Q.; Morokuma, K.; Malick, D. K.; Rabuck, A. D.; Raghavachari, K.; Foresman, J. B.; Cioslowski, J.; Ortiz, J. V.; Stefanov, B. B.; Liu, G.; Liashenko, A.; Piskorz, P.; Komaromi, I.; Gomperts, R.; Martin, R. L.; Fox, D. J.; Keith, T.; Al-Laham, M. A.; Peng, C. Y.; Nanayakkara, A.; Gonzalez, C.; Challacombe, M.; Gill, P. M. W.; Johnson, B. G.; Chen, W.; Wong, M. W.; Andres, J. L.; Head-Gordon, M.; Replogle, E. S.; Pople, J. A. *Gaussian 98*, revision A.7; Gaussian, Inc.: Pittsburgh, PA, 1998.
(43) Foresman, J. B.; Head-Gordon, M.; Pople, J. A.; Frisch, M. J. *J. Phys. Chem.* **1992**, *96*, 135.
(44) Mulliken, R. S. *J. Chem. Phys.* **1955**, *23*, 1997.
(45) Herzberg, G. *Molecular Spectra and Molecular Structure*; Van Nostrand-Reinhold: New York, 1966; Vol. III.
(46) Luth, K.; Scheiner, S. *J. Phys. Chem.* **1994**, *98*, 3582.
(47) Bader, R. F. W.; Tang, T. H.; Tal, Y.; Biegler-König, F. W. *J. Am. Chem. Soc.* **1982**, *104*, 946.
(48) Bader, R. F. W. AIMPAC series of programs, McMaster University, Hamilton.
(49) Fluder, E. M.; de la Vega, J. R. *J. Am. Chem. Soc.* **1978**, *100*, 5265.
(50) Sobolewski, A. L.; Domcke, W. *Chem. Phys.* **1998**, *232*, 257.
(51) Sobolewski, A. L.; Domcke, W. *Phys. Chem. Chem. Phys.* **1999**, *1*, 3065.
(52) Sobolewski, A. L.; Domcke, W. *J. Phys. Chem. A* **1999**, *103*, 4494.
(53) Jethwa, J.; Ouw, D.; Winkler, K.; Hartmann, N.; Vöhringer, P. *Z. Phys. Chem.* **2000**, *10*, 1367.
(54) Somorjai, R. L.; Hornig, D. F. *J. Chem. Phys.* **1962**, *36*, 1980.
(55) Mariam, Y. H.; Musin, R. N. *J. Mol. Struct.* **2001**, *549*, 123.
(56) Duschinsky, F. *Acta Physicochim. URSS* **1937**, *7*, 551.
(57) Western, C. M. *PGOPHER, a Program for Simulating Rotational Structure*; University of Bristol, http://pgopher.chm.bris.ac.uk.
(58) Marquardt, D. W. *J. Soc. Ind. Appl. Math.* **1963**, *11*, 431.
(59) Reich, J.-G. *C Curve Fitting and Modeling for Scientists and Engineers*; McGraw-Hill: New York, 1992.
(60) Sobolewski, A. L.; Domcke, W. *Chem. Phys. Lett.* **1999**, *300*, 5334.